Li_2ZrO_3-Coated NCM622 for Application in Inorganic Solid-State Batteries: Role of Surface Carbonates in the Cycling Performance

Florian Strauss,[†,*] Jun Hao Teo,[†] Julia Maibach,[‡,§] A-Young Kim,[†] Andrey Mazilkin,[†] Jürgen Janek,[†,#] and Torsten Brezesinski[†,*]

[†]Battery and Electrochemistry Laboratory, Institute of Nanotechnology, Karlsruhe Institute of Technology (KIT), Hermann-von-Helmholtz-Platz 1, 76344 Eggenstein-Leopoldshafen, Germany.

[‡]Institute for Applied Materials—Energy Storage Systems, Karlsruhe Institute of Technology (KIT), Hermann-von-Helmholtz-Platz 1, 76344 Eggenstein-Leopoldshafen, Germany.

[§]Karlsruhe Nano Micro Facility, Karlsruhe Institute of Technology (KIT), Hermann-von-Helmholtz-Platz 1, 76344 Eggenstein-Leopoldshafen, Germany

[#]Institute of Physical Chemistry & Center for Materials Science, Justus-Liebig-University Giessen, Heinrich-Buff-Ring 17, 35392 Giessen, Germany.

KEYWORDS

all-solid-state battery, Ni-rich layered oxide cathode, argyrodite solid electrolyte, surface coating, interface stability, gas evolution

ABSTRACT

All-inorganic solid-state batteries (SSBs) currently attract much attention as next-generation high-density energy storage technology. However, to make SSBs competitive with conventional Li-ion batteries, several obstacles and challenges must be overcome, many of which are related to interface stability issues. Protective coatings can be applied to the electrode materials to mitigate side reactions with the solid electrolyte, with lithium transition metal oxides, such as $LiNbO_3$ or Li_2ZrO_3, being well established in research. In addition, it has been recognized lately that carbonates incorporated into the coating may also positively affect the interface stability. In this work, we studied the effect that surface carbonates in case of Li_2ZrO_3-coated $Li_{1+x}(Ni_{0.6}Co_{0.2}Mn_{0.2})_{1-x}O_2$ (NCM622) cathode material have on the cyclability of pellet stack SSB cells with Li_6PS_5Cl and $Li_4Ti_5O_{12}$ as solid electrolyte and anode, respectively. Both carbonate-rich and carbonate-poor hybrid coatings were produced by altering the synthesis conditions. The best cycling performance was achieved for the carbonate-deficient Li_2ZrO_3-coated NCM622, due to decreased degradation of the argyrodite solid electrolyte at the interfaces, as determined by *ex situ* X-ray photoelectron spectroscopy and *in situ* differential electrochemical mass spectrometry. The results emphasize the importance of tailoring the composition and nature of protective coatings to improve the cyclability of bulk SSBs.

INTRODUCTION

Conventional Li-ion batteries (LIBs) are becoming increasingly important for application in the automotive industry.[1,2] Especially in case of electric vehicles, there is a continuous demand for improved performance concerning energy and power density, as well as safety. This has led to the renewed interest in inorganic solid-state batteries (SSBs),[3,4] which rely on the use of a solid ceramic electrolyte for ionic conduction, as opposed to the liquid electrolyte in LIBs. However, SSBs are still unable to match the performance of conventional LIBs for various reasons.

Ni-rich $LiNi_{1-x-y}Co_xMn_yO_2$, referred to as NCM or NMC, and lithium thiophosphates have been shown to hold promise as cathode active material (CAM) and solid electrolyte, respectively, for use in SSB cells.[5–9] Although lithium thiophosphates seem perfectly suited for such application, due to their high ionic conductivity and favorable mechanical properties, they suffer from relatively poor electrochemical stability.[7,10–13] This often leads to detrimental side reactions occurring at the interfaces during operation and therefore to impedance buildup and capacity fading.[14,15] An effective way to suppress, or at least mitigate, such side reactions is by applying a protective coating to the NCM secondary particles.[16–18]

In recent years, different coating chemistries and preparation approaches have been tested, with lithium transition metal oxides, such as $LiNbO_3$ or Li_2ZrO_3, being widely regarded as the most promising materials.[19–25] While these coating materials are by now routinely applied to layered oxide CAMs, thorough understanding of their working principle(s) remains elusive. Moreover, it has been shown for both $LiNbO_3$- and Li_3BO_3-based coatings, that carbonate species (always present to some extent on Ni-rich layered oxide CAMs)[26–28] may positively affect the cycling performance and stability of SSBs.[29,30]

The main objective of this work was to probe the effect that carbonates incorporated into the sol-gel derived Li_2ZrO_3 coating on NCM622 (60% Ni content) CAM have on the cyclability of bulk (pellet stack) SSB cells using argyrodite Li_6PS_5Cl, $Li_4Ti_5O_{12}$ (LTO), and Super C65 carbon black as solid electrolyte, anode, and conductive additive, respectively. In particular, we show that a carbonate-deficient Li_2ZrO_3 coating, prepared by heating at 300 °C in oxygen, leads to superior performance compared to both carbonate-rich hybrid coatings, prepared by heating at 300 or 800 °C in air, and bare NCM622, especially at higher C-rates. Using a combination of *in situ* and *ex situ* techniques provided insights into the interfacial degradation of the Li_6PS_5Cl solid electrolyte and helped to rationalize the differences in the observed cycling performance of the coated and uncoated NCM622.

EXPERIMENTAL

Solid Electrolyte Preparation

Argyrodite Li_6PS_5Cl was prepared as follows: A (non-stoichiometric) mixture of 5 g of Li_2S (Sigma Aldrich; 99+%), P_2S_5 (Sigma Aldrich; 99%), and LiCl (Alfa Aesar; 99+%)

was milled in a 250 mL zirconia jar for 1 h at 250 rpm using 10 mm diameter zirconia balls, with a ball to powder ratio of 27:1. Next, the milling speed was increased to 450 rpm, and the milling process was continued for 20 h. The recovered powder was ground using a mortar and pestle and finally heated at 300 °C for 5 h in a vacuum. The as-made solid electrolyte had a room-temperature ionic conductivity of about 1.8 mS cm^{-1}. X-ray diffraction (XRD) and Rietveld refinement patterns of the argyrodite Li_6PS_5Cl are shown in **Figure S1**.

Surface Coating of Cathode Active Material

NCM622 (BASF SE) was dried at 300 °C for 12 h in a vacuum prior to use to remove surface impurities (Li residuals).[31] To form a 1 wt.% Li_2ZrO_3 coating on the CAM particles, the NCM622 powder was dispersed in an ethanolic solution containing stoichiometric amounts of lithium and zirconium ethoxide. Lithium and zirconium ethoxide solutions were prepared by dissolving lithium metal (Albemarle Germany GmbH) or zirconium(IV) ethoxide (Sigma Aldrich; 97%) in ethanol (FUJIFILM Wako Pure Chemical Corporation; super dehydrated, 99.5+%). After stirring the dispersion for 30 min at room temperature, the ethanol was evaporated on a hot plate using an oil bath set to 90 °C. Finally, the recovered powder was dried overnight at room temperature in a vacuum, ground using a mortar and pestle, and then placed in an alumina crucible and heated for 5 h at 300 °C in air or oxygen or at 800 °C in air. Both the uncoated and coated NCM622 CAMs were stored in an argon glovebox for further use.

Cell Assembly and Electrochemical Testing

Cathode composite was prepared by mixing the Li_6PS_5Cl solid electrolyte, NCM622 CAM, and Super C65 carbon black conductive additive (TIMCAL Ltd.; pre-dried overnight at 300 °C in a vacuum) in a 3:7:0.1 weight ratio in a 70 mL zirconia jar for 30 min at 140 rpm using 10 mm diameter zirconia balls, with a ball to powder ratio of 30:1. Anode composite was prepared similarly, but using a 3:1:6 mixture by weight of carbon-coated LTO (NEI Corp.) as anode active material, Super C65 carbon black, and Li_6PS_5Cl.[32]

A custom cell setup was used for the electrochemical testing of SSBs. Assembly of 10 mm diameter pellet stack cells consisted of compressing 100 mg of Li_6PS_5Cl solid electrolyte at 125 MPa. Next, an amount of 65 mg of anode composite was pressed at 125 MPa onto the solid electrolyte pellet, followed by pressing cathode composite (10−12 mg) at 375 MPa onto the other side. A pressure of 55 MPa was maintained during electrochemical cycling. Galvanostatic (dis-)charge measurements were performed at 45 °C and at rates of C/5, C/2, and 1C (1C = 180 mA g_{NCM622}^{-1}) in a voltage range of 1.35−2.85 V vs $Li_4Ti_5O_{12}/Li_7Ti_5O_{12}$, corresponding to about 2.9−4.4 V vs Li^+/Li, using a MACCOR battery tester.

Methods

XRD measurements were conducted on samples sealed in 0.5 mm diameter borosilicate glass capillaries (Hilgenberg GmbH) using a STADI P powder diffractometer (STOE & Cie GmbH) equipped with a Cu-$K\alpha_1$ radiation source.

Scanning electron microscopy (SEM) imaging of the uncoated and coated NCM622 CAMs was done using a LEO 1530 microscope (Carl Zeiss AG) with a field emission source at 10 kV.

Transmission electron microscopy (TEM) measurements were performed on a Titan 80-300 (FEI Company) Cs image-corrected microscope at 300 kV. To protect the surface coatings from damage during focused ion beam (FIB) sample preparation and processing, nanoscale Pt layers were deposited onto the NCM622 CAM by electron- and ion beam-induced deposition. A high-angle annular dark-field (HAADF) detector was used to record scanning TEM (STEM) images.

Zirconium contents were measured *via* inductively coupled plasma (ICP) optical emission spectroscopy (OES) using both an Optima 4300 DV (PerkinElmer) and an iCAP 7600 (Thermo Scientific) spectrometer.

Attenuated total reflection (ATR) infrared (IR) spectroscopy data were collected using an ALPHA FT-IR spectrometer (Bruker) equipped with a Ge crystal in an argon glovebox.

X-ray photoelectron spectroscopy (XPS) was performed on a K-Alpha spectrometer (ThermoFisher Scientific) using a micro-focus Al-Kα X-ray source with 400 µm spot size. Data acquisition and processing, as well as curve fitting (Voigt profiles with a binding energy uncertainty of ±0.2 eV) were done employing the Thermo Avantage software.[33] For quantification, the analyzer transmission function, Scofield sensitivity factors, and effective attenuation lengths (EALs) for photoelectrons were applied.[34] EALs were calculated using the standard TPP-2M formalism.[35] Core-level spectra of the uncoated and coated NCM622 CAMs are referenced to the C 1s peak of adventitious carbon at 285.0 eV. Core-level spectra of the cathode composites before and after cycling are referenced to the Cl 2p peak at 198.8 eV of the Li_6PS_5Cl solid electrolyte. Note that the latter peak remains unaffected during sample preparation and electrochemical cycling.[15,36]

Electrochemical impedance spectroscopy (EIS) was performed at 45 °C in a frequency range of 100 mHz to 7.0 MHz with an AC voltage amplitude of 10 mV using an SP-200 potentiostat (BioLogic).

SSB cells used for *in situ* gas analysis were similar to those assembled for the electrochemical testing, except that indium foil was used as anode. Cells were assembled in a 10 mm diameter PEEK ring, by sequentially pressing the components into a pellet, before placing them in the differential electrochemical mass spectrometry (DEMS) setup.[37,38] A 9 mm diameter stainless steel mesh was placed on the cathode side to help promote connectivity and the cathode spacer had 1 mm diameter holes to ensure proper outflow of evolved gasses. Cycling was performed at 45 °C and C/20 rate in a voltage range of 2.3−3.8 V vs In/InLi, corresponding to about 2.9−4.4 V vs Li^+/Li, using a VSP-300 potentiostat (Biologic). For temperature stabilization as well as to establish a proper background for the mass spectrometer, all cells underwent a 10 h open circuit voltage period prior to cycling. The flow of helium carrier gas (2.5 mL min^{-1}; purity 6.0) was controlled by a mass flow controller (Bronkhorst; F-201CV-020-

RAD-33-Z). For gas analysis, a mass spectrometer (Pfeiffer Vacuum GmbH; OmniStar GSD 320 O2) was used. After each measurement, a calibration gas was introduced, comprising of ethylene (151.7 ± 3.0) ppm, carbon monoxide (101.3 ± 2.0) ppm, carbon dioxide (99.4 ± 2.0) ppm, nitrogen (120.4 ± 6.0) ppm, hydrogen (492.4 ± 9.8) ppm, and oxygen (50.9 ± 1.0) ppm in a helium environment (Air Liquide). See **Figures S2** and **S3** for details of the background correction and calibration procedure.

RESULTS AND DISCUSSION

Carbonate-rich and carbonate-poor hybrid surface shells were achieved by heating the Li_2ZrO_3-coated NCM622 CAM in air and oxygen, respectively. A schematic representation of the different processing steps and potential coating morphologies is shown in **Figure 1**.

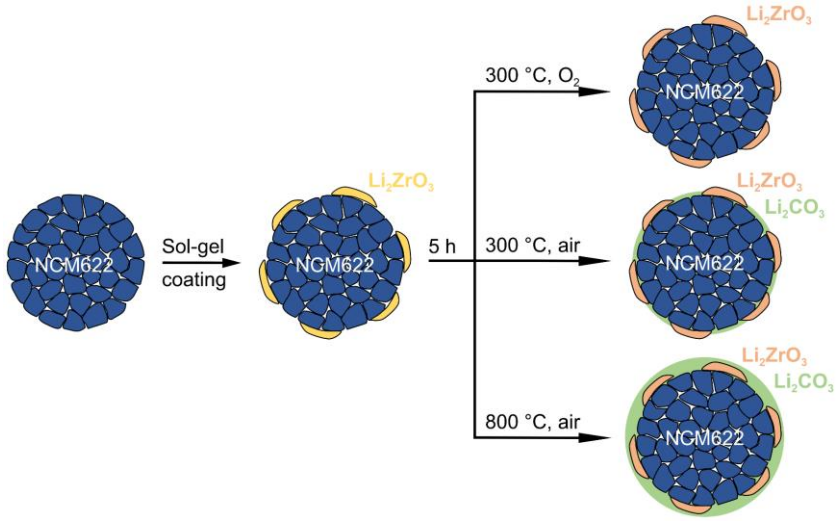

Figure 1. Schematic illustration of the formation of carbonate-rich and carbonate-poor Li_2ZrO_3-coated NCM622 CAMs.

SEM imaging of the NCM622 particles was done to probe their surface morphology before and after coating. **Figures 2a** and **b** show that the bare (uncoated) NCM622 secondary particles, with D_V^{90} = 9.0 µm, consist of primary particles up to several hundreds of nanometers in size, whose outer surface seems clean and well defined.

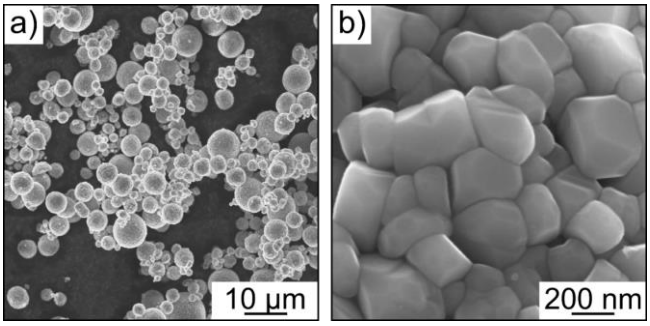

Figure 2. (a) Low- and (b) high-magnification SEM images of the uncoated NCM622 CAM.

In contrast, for the coated NCM622 CAMs, the presence of a surface shell or surface deposits can be clearly inferred from the high-magnification SEM images shown in **Figures 3a**, **c**, and **e**. To gain more insights into the coating, STEM imaging and energy dispersive X-ray (EDX) spectroscopy mapping were performed on FIB specimens. As is evident from **Figures 3b** and **d**, the Li_2ZrO_3 was indeed present as a shell after heating the coated NCM622 at 300 °C in air or oxygen. Both coatings seem relatively uniform, at least on the scale of the TEM/EDX measurements (see also low-magnification HAADF and bright-field STEM images in **Figure S4**), with thicknesses of ≤ 10 nm. The surface layer for the sample heated in air was thicker by a factor of two or so, which can be explained by the presence of carbonates. However, after heating at 800 °C in air, Zr atoms were also present in the bulk of the primary particles, due to interdiffusion into the NCM622 lattice, as can be seen in **Figure 3f**. This observation is in agreement with literature reports.[39,40] The Zr content from ICP OES measurements (**Table S1**) was found to vary from 0.60 to 0.65 wt.% or from 1.00 to 1.08 wt.% when assuming the formation of Li_2ZrO_3. This in turn suggests that the coating on the samples heated at 300 °C cannot be potentially uniform throughout the surface of the secondary particles (on the micrometer level), a result of the facile sol-gel coating process applied to the NCM622 CAM. Note that the conformality and uniformity of the coating depends strongly on the technique used, with atomic layer deposition and spray drying typically achieving the best results.[16]

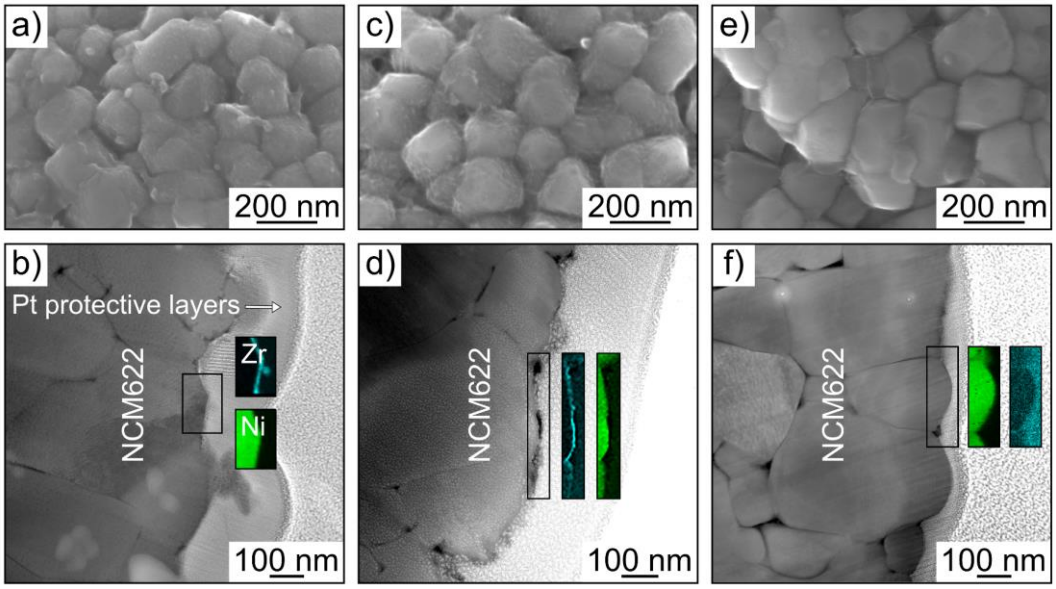

Figure 3. High-magnification SEM and HAADF STEM images of the coated NCM622 CAM heated at 300 °C in air (a and b) or oxygen (c and d) and at 800 °C in air (e and f). Insets are EDX elemental maps of the same area for Ni and Zr.

The presence of carbonates, probably Li_2CO_3, in the coatings was examined by ATR IR spectroscopy. Characteristic IR-active carbonate modes were clearly visible for the surface-treated NCM622 CAMs at 1490 and 1430 cm^{-1} (ν_3) and 870 cm^{-1} (ν_2).[41] The

very same vibrational bands were virtually absent for the bare NCM622 (**Figure 4a**). In addition, it can be seen from the spectra that the bands are more pronounced for the sample heated at 300 °C in air than oxygen. This indicates that, as expected, CO_2 (and H_2O) in the atmosphere is responsible to a large extent for the formation of carbonates on the CAM surface during heating at elevated temperatures;[30,42] however, organic residues seem to play a role too. The intensity of the vibrational bands strongly increased upon heating the coated NCM622 at 800 °C in air. Because Li_2CO_3 is known to decompose at temperatures above 720 °C,[43] we assume that the surface carbonates are primarily formed during the cooling process.

Moreover, C 1s XPS data were collected on the different NCM622 CAMs. In addition to the major peak of adventitious carbon at 285.0 eV, minor peaks centered at 288.9 and 290.1 eV were observed for the bare NCM622, due to the presence of hydrocarbon contaminants containing oxygen (C═O) and surface carbonates, respectively (**Figure 4b**).[44,45] For the coated NCM622 heated at 300 °C in air, the peak at 290.1 eV clearly increased in intensity, in agreement with the ATR IR spectroscopy data, where stronger carbonate modes were observed after heating in air than oxygen. Nevertheless, the sample heated at 800 °C in air showed the strongest carbonate peak. Apart from that, the Zr 3d XPS core-level spectra were almost identical for the coated NCM622 CAMs, showing symmetric peaks at 184.9 eV ($3d_{3/2}$) and 182.2 eV ($3d_{5/2}$), with a 2:3 area ratio (**Figure S5**). This suggests that the Zr atoms have the same or very similar local bonding environment, probably arising from amorphous Li_2ZrO_3. However, it should be noted that Li_2ZrO_3 and ZrO_2 cannot be distinguished by XPS.[40,46–51] Also, the Zr 3d peaks were much decreased for the sample heated at 800 °C in air, thereby indirectly confirming Zr interdiffusion into the NCM622 lattice.[39]

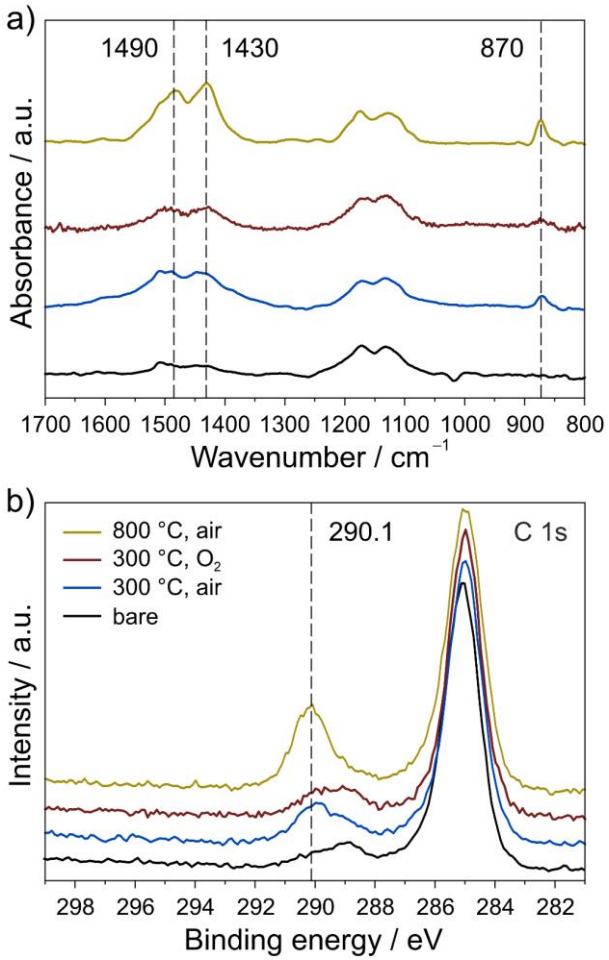

Figure 4. (a) Background-corrected ATR IR spectra of the uncoated and coated NCM622 CAMs heated at 300 °C in air or oxygen and at 800 °C in air and (b) the corresponding normalized C 1s XPS core-level spectra. The characteristic IR-active modes and XPS peak of surface carbonates are denoted.

The electrochemical performance of the coated NCM622 CAMs was tested at 45 °C and at different C-rates in pellet stack SSB cells (~10 mg_{NCM622} cm^{-2} areal loading) with argyrodite Li_6PS_5Cl and LTO as solid electrolyte and anode, respectively, and compared to that of the bare NCM622. Representative first-cycle voltage profiles at C/5 are shown in **Figure 5a**. Note that the capacity and Coulombic efficiency values given in the following are averaged over measurements on three otherwise identical cells. For the bare NCM622, specific charge and discharge capacities of 200 and 162 mAh g_{NCM622}^{-1} (~1.6 mAh cm^{-2}) were achieved in the initial cycle, corresponding to a Coulombic efficiency of 81%. Cells using the coated NCM622 heated at 300 °C in oxygen showed a comparable specific charge capacity, but delivered a larger specific discharge capacity of 170 mAh g_{NCM622}^{-1} (~1.7 mAh cm^{-2}), leading to an improved Coulombic efficiency of 85%. In contrast, for the coated NCM622 heated at 300 °C in air, both the specific charge and discharge capacities decreased to 189 and 163 mAh g_{NCM622}^{-1} (~1.6 mAh cm^{-2}) while retaining a high first-cycle Coulombic efficiency of 86%. However, the coated NCM622 heated at 800 °C in air exhibited the lowest

specific charge and discharge capacity values of 187 and 149 mAh g_{NCM622}^{-1} (~1.5 mAh cm^{-2}), as well as the lowest initial Coulombic efficiency of 80%. As can be seen from **Figure 5b**, the second-cycle Coulombic efficiencies were similar for cells using the bare or coated NCM622 heated at 800 °C in air and for cells using the coated NCM622 heated at 300 °C in air or oxygen at 95−96 and ~97%, respectively. Overall, these results suggest that only the coatings that underwent heating at 300 °C help to increase the capacity and Coulombic efficiency, especially in the initial cycles. A Zr-deficient but carbonate-rich coating on the NCM622 CAM does not lead to any performance improvement over the bare material, probably because of aggravated kinetics for charge transfer at the interfaces and/or (pronounced) formation of detrimental surface decomposition products.

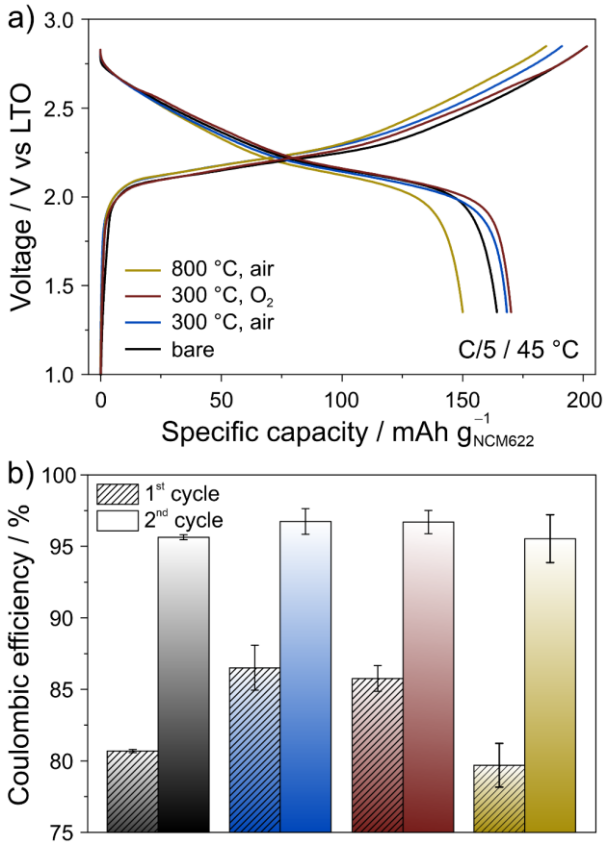

Figure 5. (a) Representative first-cycle voltage profiles of SSB cells using the uncoated or coated NCM622 CAMs heated at 300 °C in air or oxygen and at 800 °C in air and (b) the corresponding Coulombic efficiencies for the initial and second cycles. Error bars indicate the standard deviation from measurements on three cells.

In total, the cells were cycled for 60 cycles (**Figure 6a**). During the first five cycles at C/5, the coated NCM622 CAMs experienced a capacity loss of about 10 mAh g_{NCM622}^{-1}, compared to about 20 mAh g_{NCM622}^{-1} for the bare NCM622, suggesting marked degradation of the Li_6PS_5Cl solid electrolyte when using unprotected CAM. A significant drop in capacity was noticed for all cells upon increasing the C-rate to C/2 or 1C. The specific discharge capacity at 1C for the coated NCM622 heated at 300 °C in oxygen was by far the highest among the CAMs tested (e.g., 110 mAh g_{NCM622}^{-1}

versus 90 mAh g_{NCM622}^{-1} for the coated NCM622 heated at 300 °C in air). This result indicates that the heating conditions have a profound effect on the rate performance of the NCM622 in Li_6PS_5Cl-based SSB cells by affecting the composition and thickness of coating, among others. On further cycling at C/5, the different CAMs exhibited a comparable capacity fading behavior, with the coated samples heated at 300 °C in oxygen and air achieving the largest specific discharge capacities of 116 mAh g_{NCM622}^{-1} (~1.2 mAh cm^{-2}) and 107 mAh g_{NCM622}^{-1} (~1.1 mAh cm^{-2}), respectively, after 60 cycles. Cells using the bare or coated NCM622 heated at 800 °C in air were still capable of delivering about 94 mAh g_{NCM622}^{-1} (~0.9 mAh cm^{-2}) after the same number of cycles. Regarding the Coulombic efficiencies, increases upon cycling were observed for all cells, and from cycle no. 30 onward, they stabilized around 99% (**Figure 6b**). However, the rate of increase in the initial cycles was much faster for the cells using the coated NCM622 heated at 300 °C in air or oxygen, thus suggesting that less side reactions occurred.

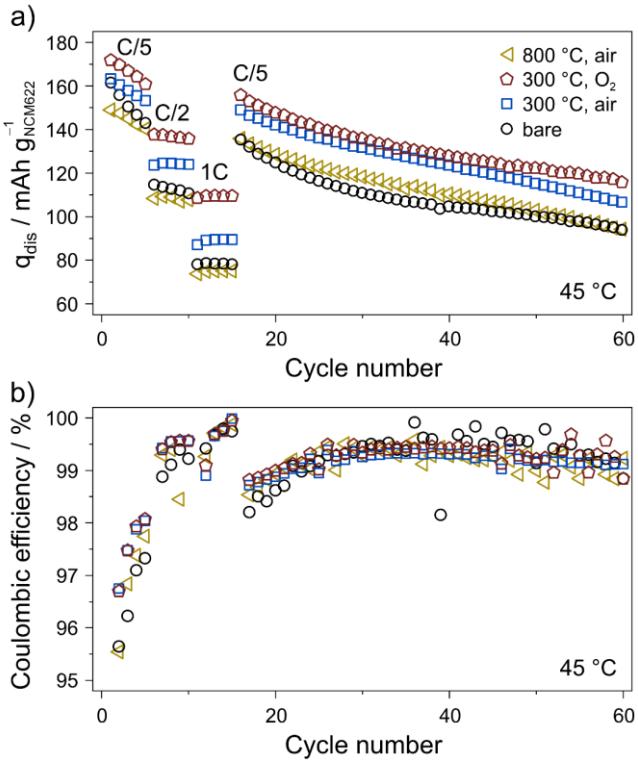

Figure 6. (a) Specific discharge capacity versus cycles for SSB cells using the uncoated or coated NCM622 CAMs heated at 300 °C in air or oxygen and at 800 °C in air and (b) the corresponding Coulombic efficiencies. All data shown are averaged from three cells.

The different cycling performance of the NCM622 CAMs tested in this work may be explained by differences in the amount and nature of solid electrolyte degradation products formed at the interfaces. Hence, XPS data were collected on the positive electrode side before and after cycling, with special emphasis placed on the S 2p and P 2p core-level regions. The pristine (uncycled) composites showed a major S 2p doublet at 161.5 eV ($2p_{3/2}$), characteristic of the PS_4^{3-} unit of Li_6PS_5Cl, and a minor

doublet at 160.3 eV, which, in principle, can be attributed both to the free S^{2-} anions in the argyrodite structure and to Li_2S impurities (**Figure S6**).[11,15,32] However, the presence of Li_2S is not apparent from the XRD pattern shown in **Figure S1**. Significant changes in the S 2p core-level spectra were noticed after the 60 cycles (**Figure 7a**), with new peaks appearing at higher and/or lower binding energies. Note that similar changes have already been observed for lithium thiophosphate solid electrolytes, thus pointing toward solid electrolyte degradation upon cycling.[11,15,52] A new doublet emerged in the binding energy region of 163.4−163.5 eV ($2p_{3/2}$) in all cases, indicating ─S─S─ bond formation (polysulfides, elemental sulfur, etc.).[11,32,52] The peaks that can generally be assigned to the free S^{2-} anions were much more prominent for both the bare and coated NCM622 heated at 800 °C in air. However, their exact origin is unclear and still under debate in literature.[11,15,53] Nevertheless, from recent studies, it seems that the formation of Li_2S is unlikely, especially when considering the voltage window used for cycling.[53] Moreover, new peaks appeared at binding energies higher than 166 eV, which we associate with the formation of SO_x. Such oxygenated sulfur species (possibly sulfites) were mainly visible for cells using the bare or coated NCM622 heated at 300 °C in air. In the other cases, only minor SO_x formation (possibly sulfites and sulfates) was apparent. Overall, it can be concluded that interfacial side reactions between the Li_6PS_5Cl solid electrolyte and the other cell components (NCM622 CAM, Super C65 carbon black additive, and Al current collector) lead to formation of polysulfides and SO_x species as solid decomposition products, in agreement with previous reports investigating lithium thiophosphate-based SSBs.[11,15,32,36]

The P 2p core-level spectra revealed a single doublet at about 131.9 eV ($2p_{3/2}$) for the pristine (uncycled) composites (**Figure S7**). After cycling, it showed distinct broadening toward higher binding energies (**Figure 7b**), due to formation of PO_x.[36,54] As expected, the new doublet at 134.1−134.2 eV ($2p_{3/2}$) was less pronounced for the coated NCM622 heated at 300 °C in air or oxygen. In summary, XPS analysis revealed that the mixed carbonate/zirconate coating on NCM622 is capable of reducing PO_x and SO_x formation to some extent, as also shown by Visbal *et al*. for a related SSB system.[54]

This finding is consistent with results from EIS measurements conducted on the cells after cycling. The worst performing NCM622 CAMs indeed showed the largest cathode interfacial resistance; a depressed semicircle was clearly observed in the Nyquist plot (**Figure S8**).

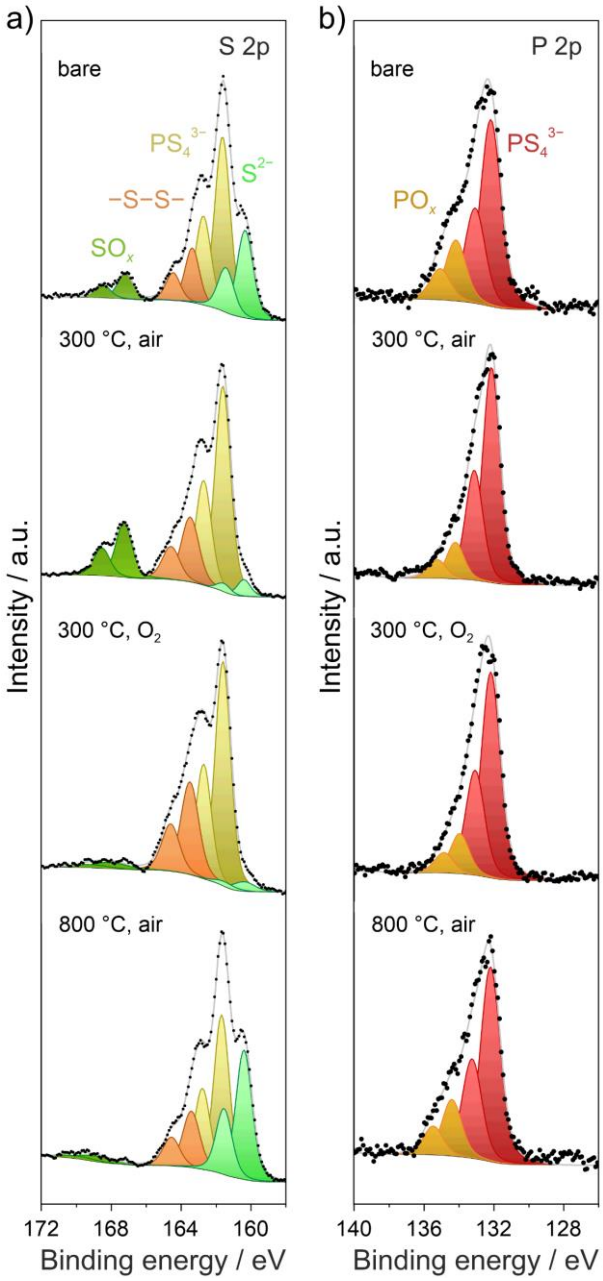

Figure 7. (a) S 2p and (b) P 2p XPS core-level spectra of the positive electrode side of cycled SSB cells using the uncoated or coated NCM622 CAMs heated at 300 °C in air or oxygen and at 800 °C in air.

In recent years, it has been shown that gaseous decomposition products can be formed as well in SSBs and the coating chemistry may affect the outgassing.[30,55,56] Hence, we decided to also study the gassing behavior in the initial cycle. To this end, cells were cycled in a custom DEMS setup in the same voltage window used for electrochemical testing while monitoring the gas evolution (mass signals from m/z = 1 to 100).[37,38] The bare NCM622 cell achieved a specific charge capacity of ~200 mAh g_{NCM622}^{-1} (**Figure 8a**), in agreement with the data shown in **Figure 5a**. Regarding the mass signal m/z = 44 (CO_2), sharp peaks were observed both at the very beginning and at the end of charge, with an onset potential of 3.6 V vs In/InLi (~4.2 V versus

Li^+/Li). While the observation of CO_2 evolution in the beginning of the initial charge cycle is usually attributed to electrochemical reduction of liquid electrolyte in conventional LIBs, this explanation can be excluded here. So far, the origin of this feature for SSBs remains largely elusive.[30,55,56] The CO_2 evolution at potentials higher than 3.6 V vs In/InLi can be associated with the electrochemical decomposition of carbonate contaminants, in agreement with literature.[26,55] In addition to CO_2 formation, a sharp peak for m/z = 32 (O_2) appeared at the end of charge (~3.8 V versus In/InLi). Although O_2 release from the NCM lattice requires the state of charge (SOC) to be greater than 80%,[57] in bulk SSBs, it has been observed for SOCs below 80%, due to inhomogeneities throughout the cathode.[56,58,59] Finally, a sharp peak for m/z = 64 (SO_2) emerged, reaching its maximum at the end of charge. This is a unique feature for lithium thiophosphate-based SSBs, and it is supposed to result from the reaction of (most likely singlet) O_2 with the solid electrolyte. Note that $^1O_2$ is released from the electrochemical decomposition of Li_2CO_3, supported by the relatively similar onset potentials of CO_2 and SO_2 evolution.[60,61] For the cell using the coated NCM622 heated at 300 °C in air, a specific charge capacity of 171 mAh g_{NCM622}^{-1} was achieved with the DEMS setup (**Figure 8b**), roughly 10% lower as compared to the data shown in **Figure 5a**. The reason for this discrepancy is unclear at present, but may be related to differences between both cell setups (applied pressure). Nevertheless, similar to the bare NCM622, both CO_2 and O_2 evolution was observed with onset potentials of 3.6 V (and at the beginning of charge) and 3.75 V vs In/InLi, respectively. However, there was no SO_2 release. For the coated NCM622 heated at 300 °C in oxygen, also solely CO_2 and O_2 evolution was observed, both with an onset potential of 3.6 V vs In/InLi (**Figure 8c**). Interestingly, the rate of CO_2 evolution was much lower than that of all other NCM622 CAMs. As to the NCM622 heated at 800 °C in air, again only CO_2 and O_2 evolution was observed, with by far the highest rate for CO_2 (**Figure 8d**). Note that we always observed additional H_2 evolution right at the beginning of the initial charge cycle (**Figure S9**), which might also explain the CO_2 evolution at the same time, as the released H_2 seems capable of somewhat reacting with the surface carbonates, thereby forming CO_2.[62]

Finally, to put all gas evolution into a broader picture, the cumulative amounts of released gasses were normalized to the specific capacity (shown for CO_2 in **Figure S10**). Both the normalized O_2 and H_2 evolution was found to be largely independent of the composition and nature of coating. In contrast, the normalized CO_2 evolution differed significantly among the CAMs tested, with the NCM622 heated at 800 °C in air showing the largest value. Interestingly, compared with the NCM622 heated at 300 °C in air or oxygen, it was higher for the bare CAM despite having a lower overall carbonate content. This is consistent with a recent report showing that carbonate-based hybrid coatings may have a positive effect on the interface stability by more effectively suppressing detrimental side reactions during cycling operation.[29,30]

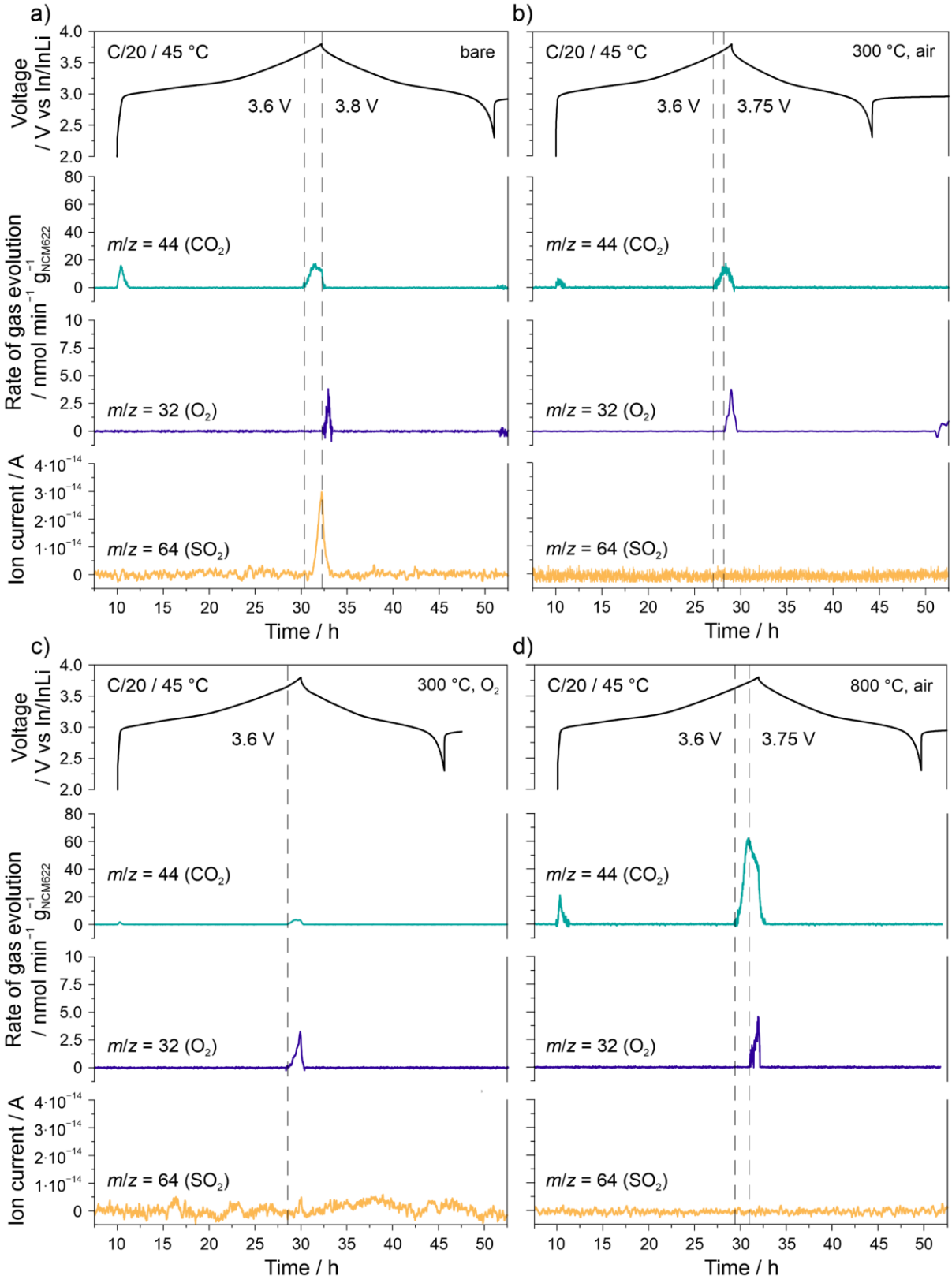

Figure 8. First-cycle voltage profiles of SSB cells using the uncoated (a) or coated NCM622 CAMs heated at 300 °C in air (b) or oxygen (c) and at 800 °C in air (d) and the corresponding CO_2 and O_2 evolution rates, as well as the ion current for SO_2 from DEMS measurements.

CONCLUSION

In summary, we have reported an investigation into Li_2ZrO_3-based coatings on NCM622 CAM for SSB applications. As recognized recently, carbonates incorporated into the protective surface layer may have a profound effect on the cycling performance. By altering the synthesis conditions concerning temperature and atmosphere, we were able to produce coatings possessing various amounts of carbonates. The best cycling performance and rate capability were achieved for the SSB cells using the Li_2ZrO_3-coated NCM622 heated at 300 °C in oxygen ("low" carbonate level), due to improved interface stability or, in other words, less degradation of the argyrodite Li_6PS_5Cl solid electrolyte, followed by the CAM heated at 300 °C in air ("medium" carbonate level). In agreement with recent reports, such coatings were capable of suppressing SO_2 evolution during electrochemical cycling. However, both CO_2 and O_2 formation and release were detected, with some dependence on the nature of coating. Overall, the results presented in this work improve the understanding of how lithium transition metal oxide-based protective coatings applied to Ni-rich NCM affect the cycling performance and stability of bulk SSBs.

ASSOCIATED CONTENT

Supporting Information

Rietveld refinement analysis of XRD data for Li_6PS_5Cl; details of the background correction and calibration procedure for DEMS; HAADF and bright-field STEM images of coated NCM622 heated at 300 °C in air; Zr 3d XPS core-level spectra of uncoated and coated NCM622; EIS spectra of cycled SSB cells; S 2p and P 2p XPS core-level spectra of uncycled cathode composites; H_2 evolution rates and normalized CO_2 evolution in the initial cycle; Zr contents.

AUTHOR INFORMATION

Corresponding Authors

*Phone: +49 721 60828907; E-mail: florian.strauss@kit.edu

*Phone: +49 721 60828827; E-mail: torsten.brezesinski@kit.edu

ORCID

Florian Strauss: 0000-0001-5817-6349

Jun Hao Teo: 0000-0002-0343-669X

Julia Maibach: 0000-0003-1339-7804

Jürgen Janek: 0000-0002-9221-4756

Torsten Brezesinski: 0000-0002-4336-263X

PRESENT ADDRESS

A.-Y.K.: Mercedes-Benz Korea Ltd., Seoul, Republic of Korea.

NOTES

The authors declare no competing financial interest.

ACKNOWLEDGEMENTS

F.S. acknowledges the Fonds der Chemischen Industrie (FCI) for financial support through a Liebig fellowship. This study was supported by BASF SE. Parts of this work were carried out with the support of the Karlsruhe Nano Micro Facility (KNMF, www.knmf.kit.edu), a Helmholtz Research Infrastructure at Karlsruhe Institute of Technology (KIT, www.kit.edu). J.H.T. is grateful to the German Federal Ministry of Education and Research (BMBF) for funding within the project ARTEMYS (03XP0114J). The authors thank Dr. Thomas Bergfeldt (KIT) for acquiring ICP OES data, Felix Walther (Justus-Liebig-University Giessen) for discussions on the XPS data analysis and interpretation, and Christian Grupe (KIT) for graphical assistance.

REFERENCES

(1) Myung, S.-T.; Maglia, F.; Park, K.-J.; Yoon, C. S.; Lamp, P.; Kim, S.-J.; Sun, Y.-K. Nickel-Rich Layered Cathode Materials for Automotive Lithium-Ion Batteries: Achievements and Perspectives. *ACS Energy Lett.* **2017**, *2*, 196–223.

(2) Sun, Y.-K. High-Capacity Layered Cathodes for Next-Generation Electric Vehicles. *ACS Energy Lett.* **2019**, *4*, 1042–1044.

(3) Janek, J.; Zeier, W. G. A Solid Future for Battery Development. *Nat. Energy* **2016**, *1*, 16141.

(4) Robinson, A. L.; Janek, J. Solid-State Batteries Enter EV Fray. *MRS Bull.* **2014**, *39*, 1046–1047.

(5) Kato, Y.; Hori, S.; Saito, T.; Suzuki, K.; Hirayama, M.; Mitsui, A.; Yonemura, M.; Iba, H.; Kanno, R. High-Power All-Solid-State Batteries Using Sulfide Superionic Conductors. *Nat. Energy* **2016**, *1*, 16030.

(6) Gao, Z.; Sun, H.; Fu, L.; Ye, F.; Zhang, Y.; Luo, W.; Huang, Y. Promises, Challenges, and Recent Progress of Inorganic Solid-State Electrolytes for All-Solid-State Lithium Batteries. *Adv. Mater.* **2018**, *30*, 1705702.

(7) Lau, J.; DeBlock, R. H.; Butts, D. M.; Ashby, D. S.; Choi, C. S.; Dunn, B. S. Sulfide Solid Electrolytes for Lithium Battery Applications. *Adv. Energy Mater.* **2018**, *8*, 1800933.

(8) Jung, S. H.; Kim, U.-H.; Kim, J.-H.; Jun, S.; Yoon, C. S.; Jung, Y. S.; Sun, Y.-K. Ni-Rich Layered Cathode Materials with Electrochemo-Mechanically Compliant

Microstructures for All-Solid-State Li Batteries. *Adv. Energy Mater.* **2020**, *10*, 1903360.

(9) Lee, Y.-G.; Fujiki, S.; Jung, C.; Suzuki, N.; Yashiro, N.; Omoda, R.; Ko, D.-S.; Shiratsuchi, T.; Sugimoto, T.; Ryu, S.; Ku, J. H.; Watanabe, T.; Park, Y.; Aihara, Y.; Im, D.; Han, I. T. High-Energy Long-Cycling All-Solid-State Lithium Metal Batteries Enabled by Silver-Carbon Composite Anodes. *Nat. Energy* **2020**, *5,* 299–308.

(10) Lee, H.; Oh, P.; Kim, J.; Cha, H.; Chae, S.; Lee, S.; Cho, J. Advances and Prospects of Sulfide All-Solid-State Lithium Batteries via One-to-One Comparison with Conventional Liquid Lithium Ion Batteries. *Adv. Mater.* **2019**, *31*, 1900376.

(11) Auvergniot, J.; Cassel, A.; Ledeuil, J.-B.; Viallet, V.; Seznec, V.; Dedryvère, R. Interface Stability of Argyrodite Li_6PS_5Cl toward $LiCoO_2$, $LiNi_{1/3}Co_{1/3}Mn_{1/3}O_2$, and $LiMn_2O_4$ in Bulk All-Solid-State Batteries. *Chem. Mater.* **2017**, *29*, 3883–3890.

(12) Richards, W. D.; Miara, L. J.; Wang, Y.; Kim, J. C.; Ceder, G. Interface Stability in Solid-State Batteries. *Chem. Mater.* **2016**, *28*, 266–273.

(13) Xiao, Y.; Wang, Y.; Bo, S.-H.; Kim, J. C.; Miara, L. J.; Ceder, G. Understanding Interface Stability in Solid-State Batteries. *Nat. Rev. Mater.* **2020**, *5*, 105–126.

(14) Koerver, R.; Aygün, I.; Leichtweiß, T.; Dietrich, C.; Zhang, W.; Binder, J. O.; Hartmann, P.; Zeier, W. G.; Janek, J. Capacity Fade in Solid-State Batteries: Interphase Formation and Chemomechanical Processes in Nickel-Rich Layered Oxide Cathodes and Lithium Thiophosphate Solid Electrolytes. *Chem. Mater.* **2017**, *29*, 5574–5582.

(15) Walther, F.; Koerver, R.; Fuchs, T.; Ohno, S.; Sann, J.; Rohnke, M.; Zeier, W. G.; Janek, J. Visualization of the Interfacial Decomposition of Composite Cathodes in Argyrodite-Based All-Solid-State Batteries Using Time-of-Flight Secondary-Ion Mass Spectrometry. *Chem. Mater.* **2019**, *31*, 3745–3755.

(16) Culver, S. P.; Koerver, R.; Zeier, W. G.; Janek, J. On the Functionality of Coatings for Cathode Active Materials in Thiophosphate-Based All-Solid-State Batteries. *Adv. Energy Mater.* **2019**, *9*, 1900626.

(17) Nakamura, T.; Amezawa, K.; Kulisch, J.; Zeier, W. G.; Janek, J. Guidelines for All-Solid-State Battery Design and Electrode Buffer Layers Based on Chemical Potential Profile Calculation. *ACS Appl. Mater. Interfaces* **2019**, *11*, 19968–19976.

(18) Xiao, Y.; Miara, L. J.; Wang, Y.; Ceder, G. Computational Screening of Cathode Coatings for Solid-State Batteries. *Joule* **2019**, *3*, 1252–1275.

(19) Ohta, N.; Takada, K.; Sakaguchi, I.; Zhang, L.; Ma, R.; Fukuda, K.; Osada, M.; Sasaki, T. $LiNbO_3$-Coated $LiCoO_2$ as Cathode Material for All Solid-State Lithium Secondary Batteries. *Electrochem. Commun.* **2007**, *9*, 1486–1490.

(20) Sakuda, A.; Kitaura, H.; Hayashi, A.; Tadanaga, K.; Tatsumisago, M. Modification of Interface Between $LiCoO_2$ Electrode and Li_2S-P_2S_5 Solid

Electrolyte Using Li_2O-SiO_2 Glassy Layers. *J. Electrochem. Soc.* **2009**, *156*, A27–A32.

(21) Ito, S.; Fujiki, S.; Yamada, T.; Aihara, Y.; Park, Y.; Kim, T. Y.; Baek, S.-W.; Lee, J.-M.; Doo, S.; Machida, N. A Rocking Chair Type All-Solid-State Lithium Ion Battery Adopting Li_2O-ZrO_2 Coated $LiNi_{0.8}Co_{0.15}Al_{0.05}O_2$ and a Sulfide Based Electrolyte. *J. Power Sources* **2014**, *248*, 943–950.

(22) Lee, J. W.; Park, Y. J. Enhanced Cathode/Sulfide Electrolyte Interface Stability Using an Li_2ZrO_3 Coating for All-Solid-State Batteries. *J. Electrochem. Sci. Technol.* **2018**, *9*, 176–183.

(23) Li, J.; Liu, Y.; Yao, W.; Rao, X.; Zhong, S.; Qian, L. Li_2TiO_3 and Li_2ZrO_3 Co-Modification $LiNi_{0.8}Co_{0.1}Mn_{0.1}O_2$ Cathode Material with Improved High-Voltage Cycling Performance for Lithium-Ion Batteries. *Solid State Ion.* **2020**, *349*, 115292.

(24) Li, X.; Jin, L.; Song, D.; Zhang, H.; Shi, X.; Wang, Z.; Zhang, L.; Zhu, L. $LiNbO_3$-Coated $LiNi_{0.8}Co_{0.1}Mn_{0.1}O_2$ Cathode with High Discharge Capacity and Rate Performance for All-Solid-State Lithium Battery. *J. Energy Chem.* **2020**, *40*, 39–45.

(25) Takada, K.; Ohta, N.; Zhang, L.; Fukuda, K.; Sakaguchi, I.; Ma, R.; Osada, M.; Sasaki, T. Interfacial Modification for High-Power Solid-State Lithium Batteries. *Solid State Ion.* **2008**, *179*, 1333–1337.

(26) Renfrew, S. E.; McCloskey, B. D. Residual Lithium Carbonate Predominantly Accounts for First Cycle CO_2 and CO Outgassing of Li-Stoichiometric and Li-Rich Layered Transition-Metal Oxides. *J. Am. Chem. Soc.* **2017**, *139*, 17853–17860.

(27) Hatsukade, T.; Schiele, A.; Hartmann, P.; Brezesinski, T.; Janek, J. Origin of Carbon Dioxide Evolved during Cycling of Nickel-Rich Layered NCM Cathodes. *ACS Appl. Mater. Interfaces* **2018**, *10*, 38892–38899.

(28) Jung, R.; Morasch, R.; Karayaylali, P.; Phillips, K.; Maglia, F.; Stinner, C.; Shao-Horn, Y.; Gasteiger, H. A. Effect of Ambient Storage on the Degradation of Ni-Rich Positive Electrode Materials (NMC811) for Li-Ion Batteries. *J. Electrochem. Soc.* **2018**, *165*, A132–A141.

(29) Jung, S. H.; Oh, K.; Nam, Y. J.; Oh, D. Y.; Brüner, P.; Kang, K.; Jung, Y. S. Li_3BO_3-Li_2CO_3: Rationally Designed Buffering Phase for Sulfide All-Solid-State Li-Ion Batteries. *Chem. Mater.* **2018**, *30*, 8190–8200.

(30) Kim, A.-Y.; Strauss, F.; Bartsch, T.; Teo, J. H.; Hatsukade, T.; Mazilkin, A.; Janek, J.; Hartmann, P.; Brezesinski, T. Stabilizing Effect of a Hybrid Surface Coating on a Ni-Rich NCM Cathode Material in All-Solid-State Batteries. *Chem. Mater.* **2019**, *31*, 9664–9672.

(31) Strauss, F.; Bartsch, T.; de Biasi, L.; Kim, A.-Y.; Janek, J.; Hartmann, P.; Brezesinski, T. Impact of Cathode Material Particle Size on the Capacity of Bulk-Type All-Solid-State Batteries. *ACS Energy Lett.* **2018**, *3*, 992–996.

(32) Strauss, F.; Stepien, D.; Maibach, J.; Pfaffmann, L.; Indris, S.; Hartmann, P.; Brezesinski, T. Influence of Electronically Conductive Additives on the Cycling Performance of Argyrodite-Based All-Solid-State Batteries. *RSC Adv.* **2020**, *10*, 1114–1119.

(33) Parry, K. L.; Shard, A. G.; Short, R. D.; White, R. G.; Whittle, J. D.; Wright, A. ARXPS Characterisation of Plasma Polymerised Surface Chemical Gradients. *Surf. Interface Anal.* **2006**, *38*, 1497–1504.

(34) Scofield, J. H. Hartree-Slater Subshell Photoionization Cross-Sections at 1254 and 1487 eV. *J. Electron Spectrosc. Relat. Phenom.* **1976**, *8*, 129–137.

(35) Tanuma, S.; Powell, C. J.; Penn, D. R. Calculations of Electron Inelastic Mean Free Paths. V. Data for 14 Organic Compounds over the 50-2000 eV Range. *Surf. Interface Anal.* **1993**, *21*, 165–176.

(36) Auvergniot, J.; Cassel, A.; Foix, D.; Viallet, V.; Seznec, V.; Dedryvère, R. Redox Activity of Argyrodite Li_6PS_5Cl Electrolyte in All-Solid-State Li-Ion Battery: An XPS Study. *Solid State Ion.* **2017**, *300*, 78–85.

(37) Berkes, B. B.; Jozwiuk, A.; Vracar, M.; Sommer, H.; Brezesinski, T.; Janek, J. Online Continuous Flow Differential Electrochemical Mass Spectrometry with a Realistic Battery Setup for High-Precision, Long-Term Cycling Tests. *Anal. Chem.* **2015**, *87*, 5878–5883.

(38) Berkes, B. B.; Jozwiuk, A.; Sommer, H.; Brezesinski, T.; Janek, J. Simultaneous Acquisition of Differential Electrochemical Mass Spectrometry and Infrared Spectroscopy Data for In Situ Characterization of Gas Evolution Reactions in Lithium-Ion Batteries. *Electrochem. Commun.* **2015**, *60*, 64−69.

(39) Schipper, F.; Bouzaglo, H.; Dixit, M.; Erickson, E. M.; Weigel, T.; Talianker, M.; Grinblat, J.; Burstein, L.; Schmidt, M.; Lampert, J.; Erk, C.; Markovsky, B.; Major, D. T.; Aurbach, D. From Surface ZrO_2 Coating to Bulk Zr Doping by High Temperature Annealing of Nickel-Rich Lithiated Oxides and Their Enhanced Electrochemical Performance in Lithium Ion Batteries. *Adv. Energy Mater.* **2018**, *8*, 1701682.

(40) Liu, S.; Dang, Z.; Liu, D.; Zhang, C.; Huang, T.; Yu, A. Comparative Studies of Zirconium Doping and Coating on $LiNi_{0.6}Co_{0.2}Mn_{0.2}O_2$ Cathode Material at Elevated Temperatures. *J. Power Sources* **2018**, *396*, 288–296.

(41) Busca, G.; Lorenzelli, V. Infrared Spectroscopic Identification of Species Arising from Reactive Adsorption of Carbon Oxides on Metal Oxide Surfaces. *Mater. Chem.* **1982**, *7*, 89–126.

(42) Kim, J.; Kim, M.; Noh, S.; Lee, G.; Shin, D. Enhanced Electrochemical Performance of Surface Modified $LiCoO_2$ for All-Solid-State Lithium Batteries. *Ceram. Int.* **2016**, *42*, 2140–2146.

(43) Kim, J.-W.; Lee, H.-G. Thermal and Carbothermic Decomposition of Na_2CO_3 and Li_2CO_3. *Metall. Mater. Trans. B* **2001**, *32*, 17–24.

(44) Hornsveld, N.; Put, B.; Kessels, W. M. M.; Vereecken, P. M.; Creatore, M. Plasma-Assisted and Thermal Atomic Layer Deposition of Electrochemically Active Li_2CO_3. *RSC Adv.* **2017**, *7*, 41359–41368.

(45) Kozen, A. C.; Pearse, A. J.; Lin, C.-F.; Schroeder, M. A.; Noked, M.; Lee, S. B.; Rubloff, G. W. Atomic Layer Deposition and in Situ Characterization of Ultraclean Lithium Oxide and Lithium Hydroxide. *J. Phys. Chem. C* **2014**, *118*, 27749–27753.

(46) Prakasha, K. R.; Sathish, M.; Bera, P.; Prakash, A. S. Mitigating the Surface Degradation and Voltage Decay of $Li_{1.2}Ni_{0.13}Mn_{0.54}Co_{0.13}O_2$ Cathode Material through Surface Modification Using Li_2ZrO_3. *ACS Omega* **2017**, *2*, 2308–2316.

(47) Ni, J.; Zhou, H.; Chen, J.; Zhang, X. Improved Electrochemical Performance of Layered $LiNi_{0.4}Co_{0.2}Mn_{0.4}O_2$ via Li_2ZrO_3 Coating. *Electrochim. Acta* **2008**, *53*, 3075–3083.

(48) Zhan, X.; Gao, S.; Cheng, Y.-T. Influence of Annealing Atmosphere on Li_2ZrO_3-Coated $LiNi_{0.6}Co_{0.2}Mn_{0.2}O_2$ and Its High-Voltage Cycling Performance. *Electrochim. Acta* **2019**, *300*, 36–44.

(49) Kong, J.-Z.; Wang, S.-S.; Tai, G.-A.; Zhu, L.; Wang, L.-G.; Zhai, H.-F.; Wu, D.; Li, A.-D.; Li, H. Enhanced Electrochemical Performance of $LiNi_{0.5}Co_{0.2}Mn_{0.3}O_2$ Cathode Material by Ultrathin ZrO_2 Coating. *J. Alloys Comp.* **2016**, *657*, 593–600.

(50) Armelao, L.; Tondello, E.; Bigliani, L.; Bottaro, G. ZrO_2 Sol-Gel Thin Films by XPS. *Surf. Sci. Spectra* **2001**, *8*, 268–273.

(51) Nisar, U.; Amin, R.; Essehli, R.; Shakoor, R. A.; Kahraman, R.; Kim, D. K.; Khaleel, M. A.; Belharouak, I. Extreme Fast Charging Characteristics of Zirconia Modified $LiNi_{0.5}Mn_{1.5}O_4$ Cathode for Lithium Ion Batteries. *J. Power Sources* **2018**, *396*, 774–781.

(52) Walther, F.; Randau, S.; Schneider, Y.; Sann, J.; Rohnke, M.; Richter, F. H.; Zeier, W. G.; Janek, J. Influence of Carbon Additives on the Decomposition Pathways in Cathodes of Lithium Thiophosphate-Based All-Solid-State Batteries. *Chem. Mater.* **2020**, *32*, 6123–6136.

(53) Ohno, S.; Koerver, R.; Dewald, G.; Rosenbach, C.; Titscher, P.; Steckermeier, D.; Kwade, A.; Janek, J.; Zeier, W. G. Observation of Chemomechanical Failure and the Influence of Cutoff Potentials in All-Solid-State Li-S Batteries. *Chem. Mater.* **2019**, *31*, 2930–2940.

(54) Visbal, H.; Aihara, Y.; Ito, S.; Watanabe, T.; Park, Y.; Doo, S. The Effect of Diamond-Like Carbon Coating on $LiNi_{0.8}Co_{0.15}Al_{0.05}O_2$ Particles for All Solid-State Lithium-Ion Batteries Based on Li_2S-P_2S_5 glass-ceramics. *J. Power Sources* **2016**, *314*, 85–92.

(55) Bartsch, T.; Strauss, F.; Hatsukade, T.; Schiele, A.; Kim, A.-Y.; Hartmann, P.; Janek, J.; Brezesinski, T. Gas Evolution in All-Solid-State Battery Cells. *ACS Energy Lett.* **2018**, *3*, 2539–2543.

(56) Strauss, F.; Teo, J. H.; Schiele, A.; Bartsch, T.; Hatsukade, T.; Hartmann, P.; Janek, J.; Brezesinski, T. Gas Evolution in Lithium-Ion Batteries: Solid versus Liquid Electrolyte. *ACS Appl. Mater. Interfaces* **2020**, *12*, 20462–20468.

(57) Jung, R.; Metzger, M.; Maglia, F.; Stinner, C.; Gasteiger, H. A. Oxygen Release and Its Effect on the Cycling Stability of $LiNi_xMn_yCo_zO_2$ (NMC) Cathode Materials for Li-Ion Batteries. *J. Electrochem. Soc.* **2017**, *164*, A1361–A1377.

(58) Bartsch, T.; Kim, A.-Y.; Strauss, F.; de Biasi, L.; Teo, J. H.; Janek, J.; Hartmann, P.; Brezesinski, T. Indirect State-of-Charge Determination of All-Solid-State Battery Cells by X-Ray Diffraction. *Chem. Commun.* **2019**, *55*, 11223–11226.

(59) Chen, K.; Shinjo, S.; Sakuda, A.; Yamamoto, K.; Uchiyama, T.; Kuratani, K.; Takeuchi, T.; Orikasa, Y.; Hayashi, A.; Tatsumisago, M.; Kimura, Y.; Nakamura, T.; Amezawa, K.; Uchimoto, Y. Morphological Effect on Reaction Distribution Influenced by Binder Materials in Composite Electrodes for Sheet-type All-Solid-State Lithium-Ion Batteries with the Sulfide-based Solid Electrolyte. *J. Phys. Chem. C* **2019**, *123*, 3292–3298.

(60) Mahne, N.; Renfrew, S. E.; McCloskey, B. D.; Freunberger, S. A. Electrochemical Oxidation of Lithium Carbonate Generates Singlet Oxygen. *Angew. Chem. Int. Ed.* **2018**, *57*, 5529–5533.

(61) Wandt, J.; Freiberg, A. T. S.; Ogrodnik, A.; Gasteiger, H. A. Singlet Oxygen Evolution from Layered Transition Metal Oxide Cathode Materials and Its Implications for Lithium-Ion Batteries. *Mater. Today* **2018**, *21*, 825–833.

(62) Lux, S.; Baldauf-Sommerbauer, G.; Siebenhofer, M. Hydrogenation of Inorganic Metal Carbonates: A Review on Its Potential for Carbon Dioxide Utilization and Emission Reduction. *ChemSusChem* **2018**, *11*, 3357–3375.

TOC GRAPHIC